Hybrid OFDM-Digital Filter Multiple Access PONs

Dong, Yixian; Giddings, Roger Philip; Tang, Jianming

Journal of Lightwave Technology

Published: 01/12/2018

Peer reviewed version

Hybrid OFDM-Digital Filter Multiple Access PONs

Y.X. Dong, R.P. Giddings, *Member, IEEE* and J.M. Tang *Member, IEEE*

***Abstract*— Hybrid OFDM-digital filter multiple access (DFMA) passive optical networks (PONs) are, for the first time, proposed and extensively investigated, where digital signal processing (DSP)-based software-reconfigurable digital filtering is employed for each individual OFDM signal from various optical network units (ONUs), and a single FFT operation and its following data recovery processes are implemented in a pipelined approach in the optical line terminal (OLT). As a direct result of combining both OFDMA and DFMA PON characteristics, the proposed hybrid OFDM-DFMA PON still maintains highly desirable features associated with DFMA PONs, more importantly, it also offers a number of unique advantages including great relaxation of digital filter DSP complexity and considerable reduction in transceiver cost, significantly enhanced upstream PON performance and its robustness and flexibility, as well as excellent backward compatibility with existing OFDM-based 4G networks. In this paper, an analytical hybrid OFDM-DFMA PON model is developed, and numerical simulations are performed to verify the validity of the proposed technique and also to examine the upstream hybrid OFDM-DFMA PON performance characteristics over representative 25km SSMF IMDD PON systems. It is shown that in comparison with the DFMA PONs, the hybrid OFDM-DFMA PON can improve the upstream ONU EVM performance by >10dB for relatively large received optical powers, and also increases the differential ONU launch power dynamic range by as large as 16dB.**

***Index Terms*— Passive optical networks (PONs), digital signal processing (DSP), digital filter multiple access, OFDM and 5G.**

I. Introduction

THE exponential growth in Internet traffic has significantly increased the demand for high bandwidth connectivity in both business and residential premises. The current global overwhelming 5G network development not only further intensifies such a tendency but also brings a number of other formidable technical challenges including dynamic reconfigurability, flexible and elastic functionality, significantly reduced system/network simplicity, as well as improved installation/operation cost-effectiveness[1]. To provide a dynamically reconfigurable, flexible, reliable, secure, transparent, smart and high-performance environment to meet these stringent requirements [1-4], it is essential to seamlessly converge traditional optical access networks, metropolitan area networks and mobile fronthaul/backhaul networks, which have been separately developed and independently operated over the past a couple of decades [5,6]. Passive optical networks (PONs) are considered worldwide as one of the most promising candidates for realizing the highly desired network convergence [2,7]. On the other hand, it is also widely envisaged that the initial stage of 5G should also have sufficient transparency to orthogonal frequency division multiplexing (OFDM)-based 4G [8,9]. As such, optical OFDM multiple access (OFDMA) PONs are expected to play a crucial role in future converged networks, as they can offer a number of well-documented salient advantages including high spectral efficiency, adaptive signal modulation according to channel characteristics, dynamic bandwidth allocation (DBA) with fine bandwidth granularity, trivial equalization through simple complex multiplication per subcarrier, as well as excellent tolerance to chromatic dispersion. For the network convergence, studies have shown that OFDMA PONs can provide high-capacity and long-reach operation [10-14]. Moreover, their performances can be further improved by non-optical carrier single-sideband [15], and their physical-layer security enhancement is also achievable when use is made of chaotic constellation transformation and pilot-aided secure key agreement [16] or three-dimension Brownian motion and chaos in cell [17].

However, OFDMA PONs have the following three major drawbacks: a) a typical OFDM signal has relatively large side lobes that result in the leakage of signal powers among different channels; b) fast Fourier transforms (FFTs) and inverse FFTs (IFFTs) implemented in very cost-sensitive optical network units (ONUs) are required to support the full subcarrier count even though individual ONUs would only be assigned a sub-set of the available subcarriers; and c) additional digital signal processing (DSP) is necessary to minimise the inter-carrier interference (ICI) effect between different upstream signals from various ONUs sharing different subcarrier subsets of an OFDM channel. Unavoidably these drawbacks considerably add the DSP complexity to ONU transceivers.

To address these technical challenges, digital filter multiple access (DFMA) PONs [18] have recently been proposed for applications in cost-effective, software defined networking (SDN) scenarios, which make use of DSP-based dynamic software-reconfigurable digital orthogonal filters to perform

This work was supported by The Ser Cymru National Research Network in Advanced Engineering and Materials under NRN024 and NRN147.

Y.X. Dong, R.P. Giddings and J.M. Tang are with the School of Electronic Engineering, Bangor University, Bangor, LL57 1UT, UK. (yixian.dong@bangor.ac.uk; r.p.giddings@bangor.ac.uk; j.tang@bangor.ac.uk).

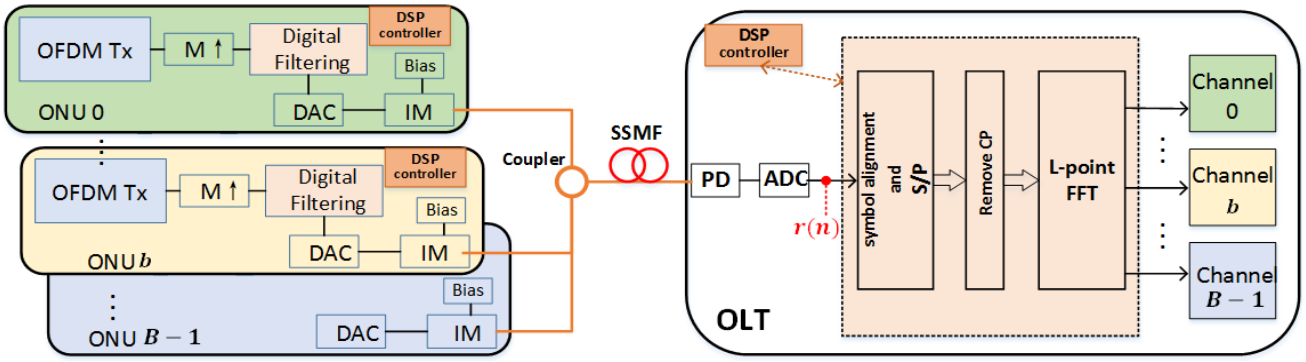

Fig. 1 Schematic diagram of the proposed hybrid OFDM-DFMA PONs simultaneously transmitting *B* ONUs over IMDD SSMFs. DAC: digital-to-analog conversion; ADC: analog-to-digital conversion; IM: intensity modulation; PD: photodetector; S/P: serial-to-parallel conversion; CP: cyclic prefix.

channel multiplexing/demultiplexing. The involved digital orthogonal shaping filters (SFs) and matching filters (MFs) are implemented in the digital domain in each individual transceiver in the ONUs and optical line terminal (OLT). Through centralized network resource abstraction and network infrastructure virtualization, the DFMA technique allows multiple independent channels of various signal modulation formats and arbitrary bandwidth granularity to transparently and dynamically share a common fiber transmission medium and other relevant network resources. Recent numerical simulations and experimental demonstrations [18,19] have shown the feasibility of utilising the technique in cost-sensitive intensity modulation and direct detection (IMDD) DFMA PON application scenarios. In addition, the physical-layer security improvement of the DFMA PONs can also be achieved by phase masking and hybrid time-frequency domain chaotic scrambling [20].

However, for an IMDD DFMA PON consisting of a larger number of ONUs, the unavoidable problem is that the number of required parallel digital filters implemented in the OLT is proportional to ONU count, as a dedicated pair of SF and MF are needed for each connection. This suggests that the corresponding DSP implementation complexity and operational expenditure may have to increase with ONU count, which is highly undesirable for cost-sensitive PONs. Moreover, in practical transmission systems, digital filtering-associated signal distortions are unavoidable due to non-perfect digital filter implementation and transmission system nonlinearity-induced imperfect digital filter orthogonality. In addition, the finite out-of-band attenuation of the digital filters also results in DFMA PONs suffering from adjacent channel interference (ACI). All the abovementioned unwanted effects constrict the practically achievable DFMA PON transmission performance.

To effectively address the abovementioned challenges associated with the IMDD DFMA PONs, in this paper, a novel technique termed hybrid OFDM-DFMA is proposed and extensively investigated, for the first time, for IMDD PONs. In an upstream hybrid OFDM-DFMA PON, regardless of the number of ONUs each having an embedded dynamic digital filter, in the OLT a single FFT operation and its following data recovery DSP processes are implemented in a pipelined way, instead of repeating these DSP functions in a parallel way for each ONU. Apart from the above unique aspects, the proposed hybrid OFDM-DFMA PONs still follow the same operating principle of the previously reported DFMA PONs in the ONU transmitter, in which the generated OFDM signals are firstly filtered by individual SFs in the digital domain, after digital-to-analogue conversion (DAC) and electrical-to-optical (EO) conversion, the passively coupled optical signal then propagates through the fiber transmission link to the OLT. In the OLT, without utilising parallel MFs, the signals from various ONUs are demultiplexed and recovered simultaneously in the digital domain by a sequence of pipelined DSP procedures described in Section II. As a direct result of combing both OFDMA and DFMA characteristics, the proposed hybrid OFDM-DFMA technique still maintains the capability of dynamic and transparent channel reconfiguration and control via the centralised SDN controller in association with the OLT/ONU-embedded DSP controllers.

More importantly, our investigations show that in comparison with the IMDD DFMA PON, the IMDD hybrid OFDM-DFMA PON can considerably improve the upstream transmission performance and differential ONU launch power dynamic range. In addition, the hybrid OFDM-DFMA PON still offers a number of salient advantages associated with the DFMA PON in terms of: a) full support of the SDN solution with network control further extended to the physical layer; b) great ease in transparent abstraction and virtualization; c) high flexibility via centralized control to dynamically realize network reconfiguration and management, and d) inherent transparency to both underlying transmission technologies and network topologies. In particular, the hybrid OFDM-DFMA PON has the unique advantages summarised below:

- Great relaxation of ONU-embedded SF DSP complexity requirement. For achieving a targeted upstream performance, the proposed technique is insensitive to SF-induced signal distortions, as discussed in Section III. This allows low complexity SFs to be implemented, thus significantly reducing the ONU cost.
- Significant simplification of the OLT DSP complexity and considerable reductions in the OLT cost. As discussed in Section III, in the upstream operation, various independent signals from different ONUs are simultaneously

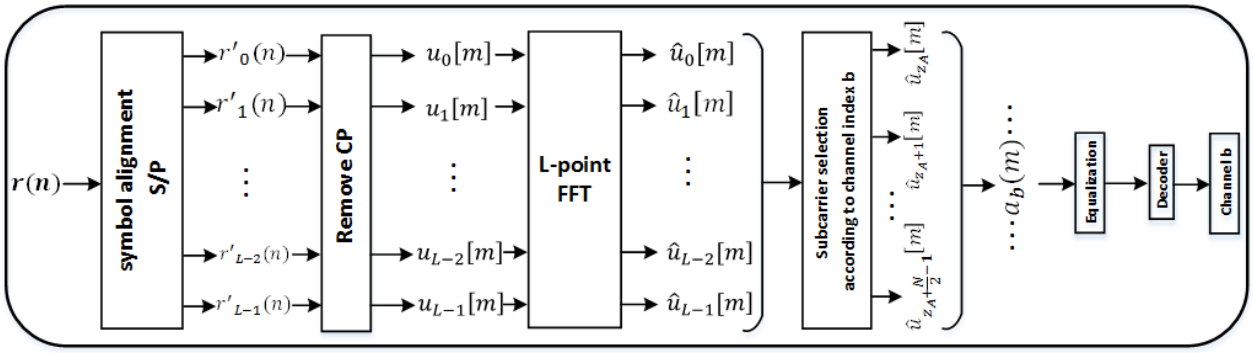

Fig. 2 Signal recovery block diagram of the hybrid OFDM-DMFA PONs.

demultiplexed and recovered with a pipelined approach. This eliminates the implementation of numerous parallel MFs and their corresponding data recovery DSP functions in the OLT. The complexity reduction is evident from the fact that, the required MF length (multiplier count) is proportional to channel count, thus total MF complexity increases in proportion to the square of channel count, whereas in the L-point FFT-based hybrid OFDM-DFMA case, multiplier count is L/2(Log_2L) with L proportional to channel count. Thus for increasing channel count the DFMA complexity will rapidly exceed the complexity in the Hybrid OFDM-DFMA case.

- Significantly enhanced upstream PON performance and its robustness and flexibility because of the proposed technique's unique feature of excellent tolerance to signal distortions and the ACI effect.
- Excellent backward compatibility with existing OFDM-based 4G networks.

In this paper, an analytical model of the hybrid OFDM-DFMA PON is developed in Section II, which offers an in-depth understanding of the operating principles of the proposed technique. In Section III, upstream transmission performances of the proposed OFDM-DFMA PON over a representative 25km standard single mode fibres (SSMF) IMDD PON are numerically explored for different application scenarios subject to various levels of signal distortion and interference. Section IV further explores other performance characteristics of the hybrid OFDM-DFMA PON in terms of differential optical launch power dynamic range and ONU count-dependent upstream performance. Finally, the paper is concluded in Section V.

II. Hybrid OFDM-DFMA Operating Principle and Theoretical Model Development

The system diagram of the proposed hybrid OFDM-DFMA PON is depicted in Fig.1, here special attention is given to the multipoint-to-point upstream operation principle only. As shown in Fig.1, the hybrid OFDM-DFMA PON conveys *B* channels each occupied by a single ONU, labelled as the 0th, 1st, 2nd… b^{th}… (B-1) th ONU, and each ONU signal is OFDM modulated. The k^{th} subcarrier of the m^{th} OFDM symbol of each channel is given by:

$$d_{k,m} = \left[R_{k,m}e^{j\theta_{k,m}}\right]h(t) \quad (1)$$

where *h(t)* is a rectangular pulse of unity amplitude and duration of one symbol period. $R_{k,m}$ is the k^{th} subcarrier's amplitude and $\theta_{k,m}$ is its phase. The m^{th} OFDM symbol is generated by the *N*-point IFFT of the set of *N* subcarriers, given by:

$$x_m(n) = \sum_{k=-\frac{N}{2}}^{\frac{N}{2}-1} d_{k,m}e^{j\frac{2\pi k(n-mN)}{L}},$$
$$k = -\frac{N}{2}, \dots, \left(\frac{N}{2}\right) - 1, m = 0,1,2, \dots \quad (2)$$

where L is the symbol length in samples. For conventional OFDM we have L=N. To generate real-valued OFDM signals, the following conditions have to be satisfied:

$$d_{-k,m} = d_{k,m}^{*}\ ,\ d_{0,m} = d_{-\frac{N}{2},m} = 0 \quad (3)$$

Thus there are $\frac{N}{2} - 1$ data-carrying subcarriers for each ONU channel.

As illustrated in Fig.1, for each ONU channel, prior to digital filtering, the process of up-sampling by a factor of M needs to be applied, which can be considered as M× over-sampling followed by multiplication by a sequence of impulses. Firstly, over-sampling by a factor of M increases the OFDM symbol length to $L = MN$ samples. The m^{th} over-sampled OFDM symbol is:

$$x'_m(n) = \sum_{k=-N/2}^{\frac{N}{2}-1} d_{k,m}e^{j\frac{2\pi k(n-mL)}{L}} \quad (4)$$

which can be rewritten as:

$$x'_m(n) = \sum_{k=-N/2}^{\frac{N}{2}-1} d_{k,m}e^{j\frac{2\pi kn}{L}}, n = mL, mL+1, \dots, mL+(L-1) \quad (5)$$

Secondly, the sequence of impulses, *s(n)*, must be spaced at *M* sample intervals, which is given by:

$$s(n) = \sum_{\tau=-\infty}^{\infty} \partial(n - \tau M) \quad (6)$$

$s(n)$ can also be expressed as a Fourier series as:

$$s'(n) = \frac{1}{M}\sum_{\beta=-\infty}^{\infty} e^{j2\pi\beta\frac{n}{M}} \quad (7)$$

where 1/M is the normalized fundamental frequency of the Fourier series. The up-sampled signal is therefore:

$$x''_m(n) = s'(n)x'_m(n) = s'(n)\sum_{k=-\frac{N}{2}}^{\frac{N}{2}-1} d_{k,m}e^{j\frac{2\pi kn}{L}}$$
$$= \frac{1}{M}\sum_{\beta=-\infty}^{\infty}\sum_{k=-\frac{N}{2}}^{\frac{N}{2}-1} d_{k,m}e^{j\frac{2\pi kn}{L}}e^{j2\pi\beta\frac{n}{M}}$$

$$= \frac{1}{M}\sum_{\beta=-\infty}^{\infty}\sum_{k=-\frac{N}{2}}^{\frac{N}{2}-1} d_{k,m} e^{j2\pi n\left(\frac{k}{L}+\frac{\beta}{M}\right)} \quad (8)$$

From Eq.(8), it can be seen that the up-sampled signal consists of multiple images where the β^{th} image is centered at a frequency of $\frac{\beta}{M}$ with β being an integer number. As an image has a bandwidth of N/L and the center frequency spacing between two neighbor images is $\frac{1}{M} = \frac{N}{L}$, the images are thus contiguous with no spectral gaps. Digital filters can therefore be used to select any image located at a desired spectral region.

As shown in Fig.1, after performing the M× up-sampling, digital filtering is then applied to the up-sampled signal. Assuming an ideal shaping filter, the b^{th} shaping filter selects the b^{th} image with its corresponding subcarriers referred to as d_{pos}, and its copy referred to as d_{neg}. Defining $d_{k,m,b}$ as the k^{th} subcarrier of the up-sampled m^{th} OFDM symbol after applying the b^{th} shaping filter, we have:

$$\sum_{k=-N}^{k=N-1} d_{k,m,b} = \{d_{neg}\}, \{d_{pos}\},$$
$$k \in [-N, N-1], m \in [1, \infty), b \in [0, B-1] \quad (9)$$

where B is the maximum number of shaping filters that can be uniformly distributed within the available spectral region, thus $B = \frac{M}{2}$. The first half of the subcarriers ($k \in (-N, -1)$) are located in the negative frequency bins, which is an exact copy of the subcarriers ($k \in (1, N-1)$) in the positive bins:

$$d_{neg} = d_{-N,m,b}, \dots d_{k,m,b}, \dots d_{-1,m,b} = d_{pos} \quad (10)$$

The subcarriers in the positive bins include the data-bearing subcarriers and their conjugates, which are:

$$d_{pos} = 0, d_{1,m,b}, \dots d_{k,m,b}, \dots, d_{N-1,m,b}$$
$$= 0, d_{1,m,b}, \dots, d_{\left(\frac{N}{2}\right)-1,m,b}, 0, d^*_{\left(\frac{N}{2}\right)-1,m,b}, \dots, d^*_{1,m,b} \quad (11)$$

Based on the above discussion, to locate the digitally filtered signal in a desired spectral region, from Eq.(8) the filtered signal can be written as:

$$x_{m,b}(n) = \frac{1}{M}\left(\sum_{k=0}^{N-1} d_{pos} e^{j2\pi n\left(\frac{k}{L}+\frac{b}{M}\right)} + \sum_{k=-N}^{-1} d_{neg} e^{j2\pi n\left(\frac{k}{L}+\frac{-b}{M}\right)}\right)$$
$$= \frac{1}{M}\sum_{k=-N}^{N-1} d_{k,m,b} e^{j2\pi n\left(\frac{k}{L}+\frac{\frac{k}{|k|}b}{M}\right)}$$
$$= \frac{1}{M}\sum_{k=-N}^{N-1} d_{k,m,b} e^{j2\pi n\left(\frac{k+bN\frac{k}{|k|}}{L}\right)} \quad (12)$$

As seen in Fig.1, the digitally filtered data sequence $x_{m,b}(n)$ is then fed to a DAC to generate an analogue electrical signal. The generated electrical signal is combined with an optimum DC bias current to drive an optical intensity modulator. After that, different optical signals from various ONUs are passively combined in an optical coupler located at the remote node to generate an aggregated upstream optical signal that propagates to the OLT.

To obtain a simple analytical solution capable of offering an overall view of the proposed hybrid OFDM-DFMA technique, linear transmission systems are assumed in this section, and numerical simulations are performed in Section III to examine the feasibility of the proposed technique in practical non-linear PON transmission systems. As a direct result of the linear system assumption, the passively coupled signal from B ONUs can be expressed as:

$$y(n) = \sum_{b=0}^{B-1} x_{m,b}(n)$$
$$= \sum_{b=0}^{B-1}\left(\frac{1}{M}\sum_{k=-N}^{N-1} d_{k,m,b} e^{j2\pi n\left(\frac{k+bN\frac{k}{|k|}}{L}\right)}\right)$$
$$= \frac{1}{M}\left(\sum_{b=0}^{B-1}\sum_{k=-N}^{N-1} d_{k,m,b} e^{j\frac{2\pi\left(k+bN\frac{k}{|k|}\right)n}{L}}\right) \quad (13)$$

Let $\rho = k + bN\frac{k}{|k|}, k \in [-N, N-1], b \in [0, B-1], \rho \in [-BN, BN-1]$, so the above combined signal becomes:

$$y(n) = \frac{1}{M}\sum_{\rho=-BN}^{BN-1} d_{m,\rho} e^{j\frac{2\pi\rho n}{L}}, d_{m,\rho} = d_{k,m,b} \quad (14)$$

Eq.(14) indicates that the combined signal can be considered to be produced by the L-point IFFT operation with L= 2BN. As such, in the OLT, the L-point FFT can be applied to $y(n)$ to recover the sequence $d_{k,m,b}$, which can be expressed as:

$$d_{k,m,b} = \sum_{\rho=0}^{2BN-1} r(n) e^{-j\frac{2\pi\rho n}{L}}, k \in [-N, N) \quad (15)$$

where $r(n)$ is the received signal after the ADC in the OLT, as seen in Fig.1, and $r(n)$ is given by:

$$r(n) = Cy(n) \quad (16)$$

where C is the scale factor accounting for the signal power variation in the linear system. Here it is also worth noting that the DC component is not included in the analysis, as such a component is removed completely and immediately after O-E conversion.

The signal emerging from the ADC passes through a deserialiser to provide parallel signal samples corresponding in length to one symbol period, but arbitrarily located and so not aligned to the symbol boundaries. A symbol alignment block is employed to achieve symbol alignment and compensate for any possible symbol offset. This can be undertaken using synchronisation techniques similar to OFDMA-PONs [14, 21]. As shown in Fig.2, after the symbol alignment and S/P conversion of the received signal $r(n)$, the sample sequence $\{r'_z(n)\}$is obtained. The cyclic prefix (CP) can then be removed as it has no useful data, thus the remaining L time-domain samples are obtained for each symbol, which is expressed as $u_0[m], u_1[m] \dots u_{L-1}[m]$ in Fig.2. After performing the L-point FFT operation, the output sample sequence $\hat{u}_0[m], \hat{u}_1[m], \dots, \hat{u}_z[m], \dots, \hat{u}_{L-1}[m], z \in [0, L-1]$ is obtained, which is exactly the reverse replica of Eq.(15).

In the sequence of $\{\hat{u}_z[m]\}, z \in [0, L-1]$, the first half of the sequence ($z \in [0, \frac{L}{2}-1]$) corresponds to the positive frequency bin d_{pos}, and the lowest frequency starts from $z = 0$. Whilst the second half ($z \in [\frac{L}{2}, L-1]$)) corresponds to the negative frequency bin d_{neg}, which is the copy of d_{pos}. Theoretically speaking, the subcarriers located in either d_{pos}or d_{neg} can be selected to recover the targeted signal in the b^{th} ONU channel $a_b(m)$. To obtain the best results from $\{\hat{u}_z[m]\}$,

Eq.(17) is utilized, which presents the rules of the subcarrier selection, and the corresponding subcarrier index z is given in Eq.(18):

$$a_b(m) = \begin{bmatrix} \overbrace{\hat{u}_z[m], \hat{u}_{z+1}[m] \dots, \hat{u}_{z+\frac{N}{2}-1}[m]}^{the\ first\ and\ \frac{N}{2}-1\ data-bearing\ subcarriers} \\ \underbrace{\hat{u}_{z+N-1}[m], \hat{u}_{z+N-2}[m], \dots, , \hat{u}_{z+\frac{N}{2}}[m]}_{\frac{N}{2}\ conjugate\ subcarriers} \end{bmatrix}, \quad b = 0,1, \dots, B-1 \quad (17)$$

$$z = \begin{cases} 0, & b = 0 \\ \frac{L}{2} + (B - b - 1) \cdot N, & b \geq 1 \end{cases} \quad (18)$$

where b is the channel index for the b^{th} ONU channel and B is the total number of ONU channels. Thus the recovered signal from the b^{th} channel is identified, which is then followed by further equalization and decoding operations. The equalization process is the standard OFDM equalization as reported in [14,18]. For simplicity without losing any generality, the ideal shaping filters are applied in the above described mathematical derivations, though other non-ideal shaping filters mentioned below are also applicable, and their distortions can be recovered by the following equalization process. Filter parameters optimizations are discussed in Section III.

From the above analysis, it can be seen that without implementing numerous parallel MFs, the OLT simultaneously recovers the signals from different ONUs utilizing a single L-point FFT operation. Here it is also worth emphasizing the following two aspects:

- Any orthogonal digital filter construction approaches such as the Hilbert-pair approach [18] and the Gaussian approach [22] are applicable for the hybrid OFDM-DFMA PONs. When the Hilbert-pair approach is adopted, from the transceiver complexity point of view, the same type (either quadrature-phase or in-phase) of the digital filters at different RF central frequencies are preferable, which, however, halves the maximum achievable signal transmission capacity for a fixed DAC/ADC sampling speed. Such a technical problem can be solved when use is made of the Gaussian approach [22].
- The digital filtering and the FFT operation are controlled and managed using DSP controllers embedded in the ONUs and the OLT, respectively, as shown in Fig.1. To establish a reconfigurable and elastic connection, according to transmission system frequency response characteristics and network traffic status, the centralized SDN controller works together with the embedded DSP controllers to dynamically set optimum digital filter coefficients and map each individual channel with its corresponding subcarriers of the L-point FFT operation.

TABLE I
LIST OF PARAMETERS

PARAMETER	VALUE	PARAMETER	VALUE
DAC/ADC sample rate	12.5 GS/s	DAC/ADC resolution	8 bits
Clipping ratio	13dB	Cyclic Prefix	25%
Modulation formats	16QAM	Total number of IFFT points of each channel	32
Transmitted optical power	0dBm	Received optical power	-2dBm
SSMF length	25km	Up sampling factor M	4
PIN detector bandwidth	12.5GHz	PIN detector sensitivity/ responsibility	-19dBm /0.99
Fiber dispersion	17 ps/nm/km	Fiber dispersion slope	0.07 ps/nm/km
Fiber Kerr coefficient	2.35e-20 m^2/W	Fiber loss	0.2 dB/km
SF/MF filter length range	2/8/16/32	Hybrid OFDM-DFMA FFT size	128

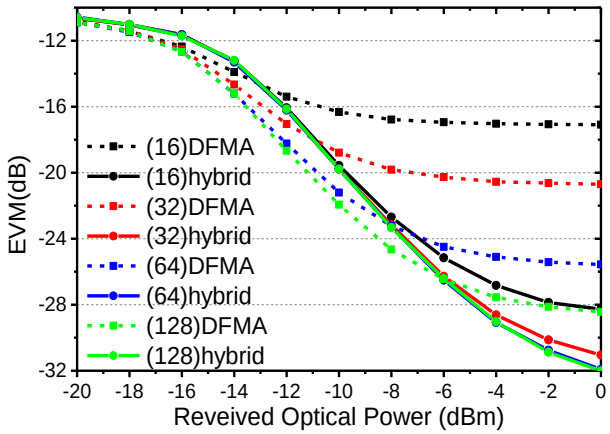

Fig.3 EVM of ONU 1 versus received optical power with different digital filter tap-counts for both the hybrid OFDM case and DFMA case.

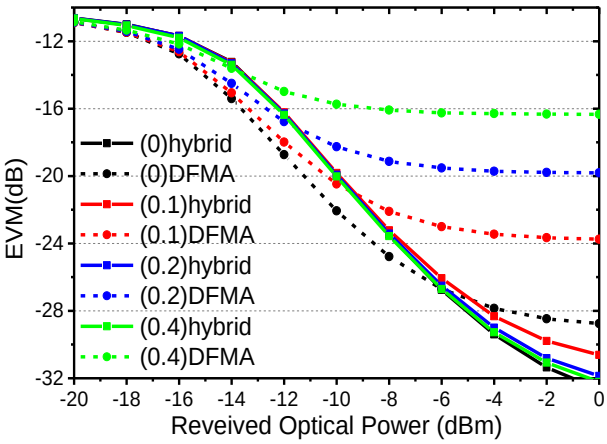

Fig.4 EVM of ONU 1 versus received optical power with different excess of bandwidth parameters (alpha value) for hybrid OFDM and DFMA.

III. HYBRID OFDM-DFMA PON VERIFICATION AND OPTIMUM FILTER DESIGN

To evaluate the validity of the theoretical model derived in Section II, and to explore the performance characteristics of the proposed hybrid OFDM-DFMA PON, numerical simulations of the upstream performances of 25 km SSMF IMDD hybrid OFDM-DFMA PON are undertaken in this section. Signal generation and detection are simulated using MATLAB and the optical fibre transmission is simulated using VPI Transmission maker. To highlight the upstream hybrid OFDM-DFMA PON performance, comparisons are also made to the DFMA PON

with corresponding MFs in the OLT (abbreviated as 'DFMA' case).

To simulate OFDM signal generation and detection, the approach reported in [23] is adapted. Throughout the paper, each ONU is assigned a whole OFDM channel, with each channel consisting of fifteen, 16-QAM modulated, data-bearing subcarriers (N=32). In each ONU, an ideal optical intensity modulator is utilised, which produces an optical field signal $S_o(n)$, having a waveform governed by $S_o(n) = \sqrt[2]{y'(n)}$, here $y'(n) > 0$ is the electrical driving current of the signal with an optimum DC bias current being added. Apart from simplicity, the utilisation of the ideal optical intensity modulator can also completely eliminate the optical beat interference (OBI) effect [24]. For practical upstream IMDD PON systems, the OBI effect is negligible when the optical wavelength spacing between adjacent ONUs is larger than the threshold experimentally identified in [24].

For simplicity, here two ONUs are considered in the adopted multipoint-to-point upstream PONs. The construction of the digital filters in the ONUs is undertaken using the Hilbert-pair approach [18], in which the baseband pulse $p(t)$ has a square-root raised-cosine form and the central frequency f_k corresponds to the RF central frequency of the Hilbert-pair. Each Hilbert-pair includes both in-phase and quadrature-phase filter components to support two spectrally-overlapped orthogonal channels. In this paper, for both ONU1 and ONU2, only the in–phase filters are utilised at different RF central frequencies governed by Eq.(19):

$$f_k = (2k+1)\frac{f_s}{2M}, k = 0,1,\dots,B-1 \qquad (19)$$

where f_s is the DAC/ADC sampling speed. The central frequencies are chosen to uniformly distribute the filter frequency responses within the available spectral region determined by the DAC/ADC sampling speeds. To accommodate the two ONUs in the entire spectral region, the up-sampling factor M is taken to be 4, $f_1 = f_s/8$, $f_2 = 3 \times f_s/8$, and all other simulation parameters are listed in Table I. For each case considered, identical parameters are applied to both the hybrid OFDM-DFMA PON and the DFMA PON.

For each ONU, the achievable signal bit rate, R_b ,can be calculated using the formula below:

$$R_b = \frac{f_s \sum_{k=1}^{N_s} n_{kb}}{2(N_s+1)(1+C_p)M} \qquad (20)$$

where n_{kb} is the number of binary information bits conveyed by the k-th subcarrier within one OFDM symbol period, $N_s = \frac{N}{2} - 1$ is the total number of data-bearing subcarriers and $C_p$is the overhead parameter associated with the cyclic prefix and training sequence. By utilising the parameters listed in Table I, a signal bit rate of 4.7Gb/s can be easily calculated for each ONU. Eq.(20) also shows that, for a fixed DAC/ADC sampling speed, increasing the up-sampling factor decreases proportionally the signal bit rate of each ONU, although the total maximum capacity of the PON can be maintained.

From Table I, it can be seen that the IFFT size for generating the OFDM signal by each ONU is *N*=32, and the up-sampling factor *M* is 4, thus in the OLT of the hybrid OFDM-DFMA PON, there are *L*=128 samples per symbol applied to the FFT operation after the S/P conversion. From Eq.(17) and Eq.(18) it can also be seen that the samples of subcarrier index 1-16 (the first and 15th data-bearing subcarriers) from ONU1 are located in the sequence $\hat{u}_0, \hat{u}_1 .., \hat{u}_{15}$, and the sequence $\hat{u}_{64}, \hat{u}_{65} .., \hat{u}_{79}$ is selected to construct the data-bearing subcarriers for ONU2. Thus, after equalization and decoding, the two signals from both ONUs are recovered.

Under the above numerical simulation conditions, the ONU1 error vector magnitude (EVM) versus received optical power (ROP) performances of both the hybrid OFDM-DFMA and DFMA PONs are presented in Fig.3 for different digital filter tap counts. The FEC limit of 1.0E-3 is considered, which corresponds to -17dB EVM (or 14%) [25]. Fig.3 shows that the proposed hybrid OFDM-DFMA PON can reach EVMs of -17dB when ROPs are higher than -12dBm. This indicates that the proposed technique works well for both linear and non-linear IMDD PON systems, thus the feasibility of the proposed hybrid OFDM-DFMA technique is confirmed. Moreover, when varying digital filter tap counts between 16, 32, 64 and 128, the proposed hybrid OFDM-DFMA PON performances are very robust to the variations in filter tap

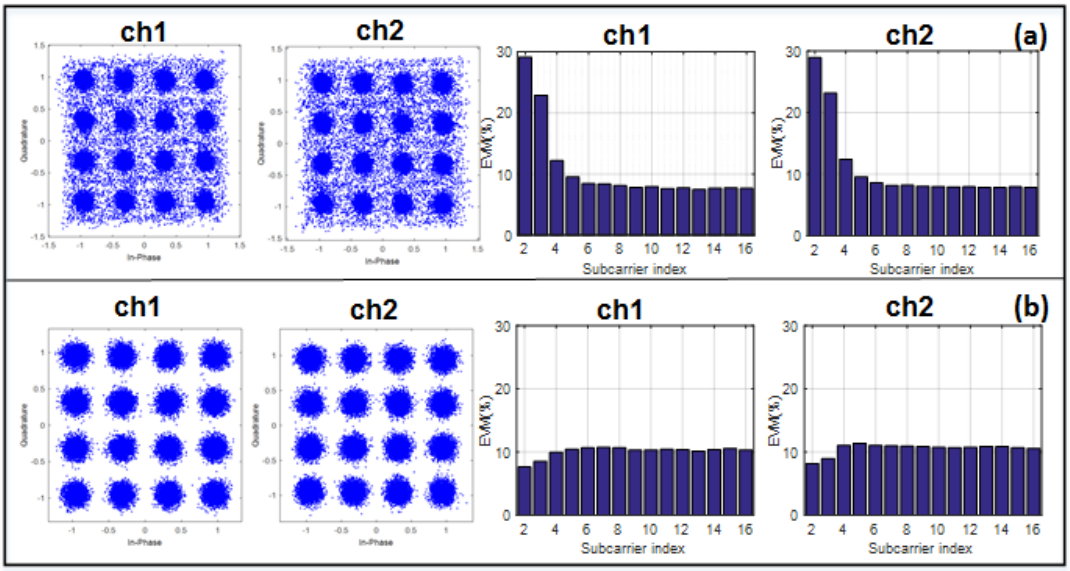

Fig. 5 Constellations and EVM distribution among all subcarriers, (a) DFMA case, (b) hybrid OFDM case.
(Note: subcarrier index=1 corresponds to the unused DC frequency)

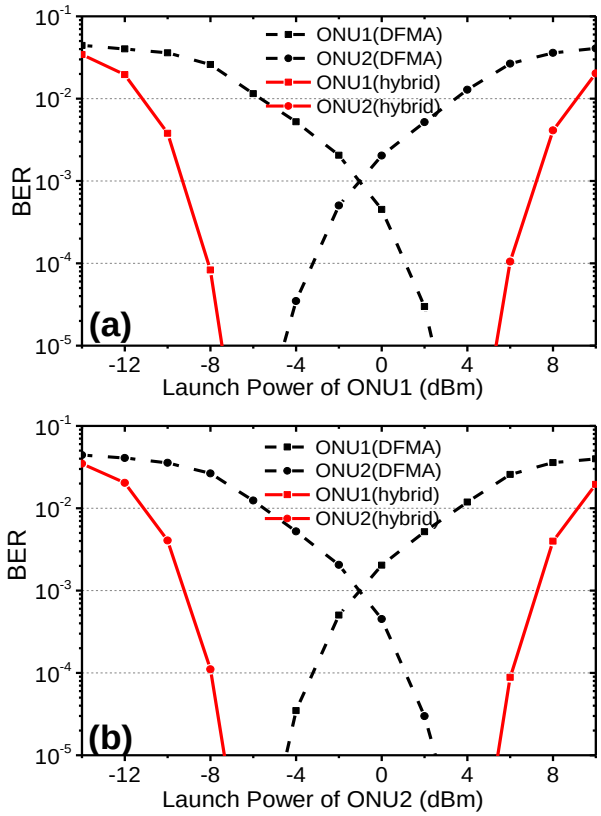

Fig.6 BER performance versus ONU optical launch power. (a) power-varying ONU1, (b) power-varying ONU2. The black curves refer to the DFMA PON, the red curves refer to the hybrid OFDM-DFMA PON.

count. On the contrary, the DFMA PON performances significantly depend on filter tap count, especially over the noise floor region. This is because the finite tap count-induced non-flat frequency response of the digital filter leads to signal distortions: the filter frequency response ripple variation range and associated signal distortions increase with decreasing the number of taps. The DFMA PONs suffer stronger imperfect filter impairments as both the SFs and MFs are implemented in the ONUs and OLTs respectively, whilst the hybrid OFDM-DFMA PONs are free from the OLT-embedded MFs, thus introducing less signal distortions. This results in the hybrid OFDM-DFMA EVM curves almost perfectly overlapping for different tap counts, as shown in Fig.3.

Such a feature reveals that in comparison with the DFMA PON, the proposed hybrid OFDM-DFMA PON is less sensitive to imperfect digital filter-induced signal distortions. For achieving the same transmission performance, the proposed technique not only permits lower digital filter complexity but also significantly enhances the PON robustness and flexibility. Such a statement is further signified by the performance for the 16 tap count case, where the noise floor in the hybrid OFDM-DFMA PON is significantly lower than the DFMA PON with the filter taps as large as 64. In addition, for a specific filter tap count and over relatively low ROPs, the DFMA PON performance is slightly better than the hybrid OFDM-DFMA PON, the ROP corresponding to such performance cross-point between two PON technologies increases with increasing filter count, as shown in Fig.3. This is because the DFMA-associated MFs can reduce the system noise effect. In Fig.3, only ONU1 performance is presented, because ONU2 employs the identical digital filter parameters, except that ONU2 operates at a higher RF frequency. Our numerical simulations show that for the same simulation conditions, the performance of ONU2 is very similar to ONU1. This suggests that the hybrid OFDM-DFMA PON performance is independent of ONU spectral allocation.

Fig. 4 presents the ONU1 EVM versus ROP for different levels of ACI. Here the different ACI levels are introduced by varying the filter's alpha parameter [18], which controls the excess of bandwidth with respect to the minimum bandwidth determined by the symbol period. Generally speaking, for a given filter tap count, a larger alpha value produces lower in-band frequency response ripples, but gives rise to larger filter response side lobes, thus leading to greater ACI. When numerically simulating Fig. 4, the alpha parameter values are taken to be 0, 0.1, 0.2 and 0.4, and the tap counts are fixed at 128 to minimise the finite tap count-induced signal distortions. All other simulation parameters are kept the same as those adopted in Fig.3.

It can be seen in Fig. 4 that the proposed hybrid OFDM-DFMA PON performances are almost independent of ACI level. In sharp contrast, the performance of the DFMA PON varies considerably with ACI level, in particular over the noise floor region. The physical mechanism underlying such observed behaviour is the system nonlinearity-induced imperfect orthogonality between the SFs and MFs, which means that the DFMA-embedded MFs cannot fully reject the leaked signal power from its adjacent channels, and due to the filter's excess of bandwidth some adjacent channel power aliases into the wanted signal after down-sampling. However, for the hybrid OFDM-DFMA PON, the system nonlinearity gives each SF the same effect, thus the power leakage from the adjacent channels is largely rejected by the single FFT operation and its following data recovery process. As such the hybrid OFDM-DFMA PON mainly suffers from out-of-band channel leakage due to the finite out-of-band attenuation of the SFs. These behaviours clearly demonstrate that the proposed technique is highly tolerant to ACI. The existence of the performance cross-points between the hybrid OFDM-DFMA PON and the DFMA PON is very similar to that observed in Fig.1.

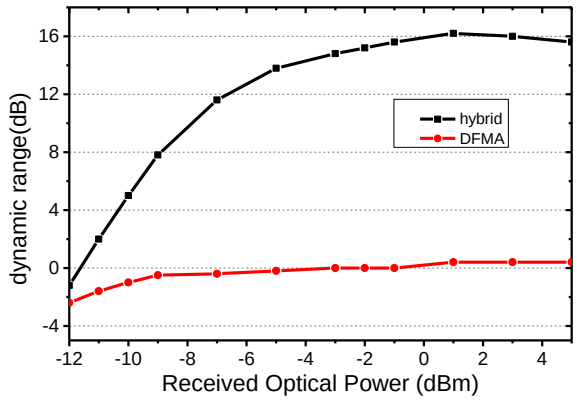

Fig.7 Optical launch power dynamic range of ONU1 as a function of received optical power

To further explore the proposed technique's robustness against the ACI effect, the overlaid and equalised combined constellations and subcarrier EVM distributions for both ONUs are plotted in Fig. 5 (a) and (b) for the DFMA PON and the hybrid OFDM-DFMA PON, respectively. Here the ROPs are fixed at -10dBm, and the tap count and the alpha parameter value are taken to be 128 and 0.2 respectively. These parameters give rise to the FEC limit of EVM of -17dB or 14% [25] for the DFMA PON, as shown in Fig.4. As a direct result of the large alpha parameter value-induced enhancement in the ACI effect, and given the fact that lower frequency subcarriers are located at the edges of the frequency band, the first two subcarriers of both ONU channels are almost destroyed in the DFMA PON, as seen in Fig.5(a). However, in the hybrid OFDM-DFMA PON, shown in Fig. 5(b), these two low frequency subcarriers are hardly affected by the ACI effect, leading to almost flat EVM distributions across all the subcarriers. In comparison with the DFMA PON, the superior ACI rejection capability associated with the hybrid OFDM-DFMA PON is further evidenced by its corresponding clear constellations, illustrated in Fig.5(a) and Fig.5(b).

In summary, the excellent performance of the hybrid OFDM-DFMA PONs not only validates the proposed technique for use in the application scenarios of interest of the paper, but also demonstrates the hybrid OFDM-DFMA PON's unique advantages over the DFMA PONs in terms of upstream transmission performance improvement, digital filter complexity reduction and increased tolerance to signal distortions and ACI caused by the finite tap count-induced digital filter imperfection and system nonlinearity.

IV. Hybrid OFDM-DFMA PON Upstream Performance Characteristics

A. Differential ONU Launch Power Dynamic Range

The hybrid OFDM-DFMA performance robustness to differential ONU launch power is examined in Fig. 6, where the BER performance of a power-varying ONU is plotted as a function of its optical launch power, whilst the other fixed-power ONU's launch power is kept constant at -1dBm. For simplicity but without losing generality, here just two ONUs are considered and the ROP in the OLT is fixed at -2dBm. The digital filters have 32 taps, and the alpha parameters are set at 0 to allow fair comparison with the

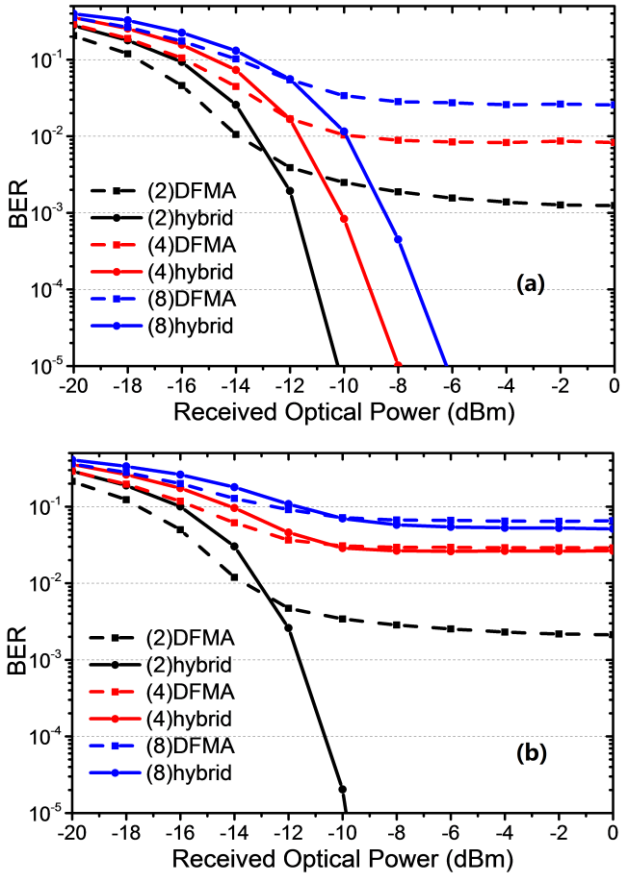

Fig.8 BER versus received optical power in multiple ONU cases when filter tap count is 32, (a) channel 1; (b) channel 2.

previous performances presented in Fig.3. All other parameters are identical to those listed in Table I.

As expected, an increase in optical launch power from one ONU improves its own BER performance, but simultaneously degrades the BER performance of the other ONU, as shown in Fig. 6 (a) and (b). This mainly results from the opposite changes in effective optical signal to noise ratio (OSNR) experienced by these ONUs. In this context, the differential ONU launch power dynamic range is defined, for a fixed ROP in the OLT, as the maximum allowable variation range of optical launch power from a specific ONU, over which the total BERs of all individual ONU signals simultaneously transmitted over the PON are still less than the adopted FEC limit.

At an ROP of -2dBm, the differential launch power dynamic range of the DMFA PON is virtually 0dB, however for the hybrid OFDM-DFMA PON, the differential launch power dynamic range of both ONU1 and ONU2 significantly increases to 16dB. Such a huge improvement mainly results from the excellent tolerance of hybrid OFDM-DFMA to the low filter tap count-based imperfect filter-induced signal distortions. The hybrid OFDM-DFMA-enhanced differential ONU dynamic range also brings improved PON performance robustness.

The ROP-dependent differential launch power dynamic range characteristics are explored in Fig.7, where ONU1 is power-varying with all other parameters kept identical to those adopted in Fig.6. It is shown in Fig.7 that for the DFMA PON, the differential launch power dynamic range is always around

0dB, whilst for the hybrid OFDM-DFMA PON, the dynamic range increases almost linearly from 0dB to 16dB when ROPs increasing from -12dBm to 1dBm, beyond which the differential launch power dynamic range plateaued at around 16dB. The flattening of the differential launch power dynamic range to a maximum value is mainly attributed to nonlinearities and noise associated with the transmission channel. As expected from Fig.6, the same ROP-dependent differential launch power dynamic range characteristics also hold when ONU2 power varies. In addition, at an ROP of around -11.5dBm, the hybrid OFDM-DFMA dynamic range is 0dB, indicating that both channels reach the FEC limit at the same time, which is in agreement with that in Fig.3, where the corresponding EVM is -17dB for the 32-tap case. Meanwhile for the DFMA PON, the corresponding dynamic range value is negative when ROPs are lower than -1dBm, this means both of the two channels fail to operate below the FEC limit.

B. ONU Count-Dependent Performance

Having demonstrated the effectiveness of the hybrid OFDM-DFMA PON in improving differential launch power dynamic range for the two ONU case, this subsection further extends the application scenario to multi-ONU hybrid OFDM-DFMA PONs.

The ONU count-dependent hybrid OFDM-DFMA PON performance is examined in Fig.8, where for each case considered, equal ONU launch powers and a constant total optical launch power of 0dBm are always used at the remote node, and the up-sampling factors are twice the total number of ONUs simultaneously accommodated, i.e., $M=2B$. Here the tap count is fixed at 32 and the alpha parameter is set at 0.1 to provide a practically achievable trade-off between side lobes and in-band frequency response ripples. Each ONU is located at a dedicated RF central frequency governed by Eq. (19). Other adopted simulation parameters are identical to those utilised in previous sections.

The BER performances of ONU1 and ONU2 as a function of ROP are plotted in Fig.8 (a) and Fig.8 (b) respectively, where the total number of ONUs varies from 2 to 8. It can be seen in Fig.8 (a) that in the DFMA PON, both ONU1 and ONU2 fail to reach the FEC limit of 1E-3 over the entire ROP variation range. However, in the hybrid OFDM-DFMA PON incorporating 2/4/8 ONUs, ONU1 reaches the FEC limit at -12/-10/-8dBm respectively. Furthermore, for each case considered, the hybrid OFDM-DFMA PON has a significantly lower noise floor than the corresponding DFMA PON. This manifests from the fact that ONU1 suffers smaller interference from other ONUs. Here it is also worth mentioning that when the number of ONUs is doubled, as observed in Fig.8 (a), the effective signal power from each ONU is decreased by 1.5dB (half of 3 dB in the electrical domain) rather than the value of 2dB. The 0.5 dB difference is mainly contributed by the multiple access interference (MAI) effect [26].

It is observed in Fig.8 (b) that ONU2 in the hybrid OFDM-DFMA PONs incorporating 4 and 8 ONUs fail to reach the adopted FEC limit and tend to have similar performances compared to the corresponding DFMA PONs. This is because the crosstalk effects from other ONUs are extremely large for the adopted digital filter parameters. The fixed filter tap count of 32 gives rise to a filter length of 4 (2) for the 4-ONU (8-ONU) case. As the filter length corresponds to the number of non-zero samples that a SF processes at any time, for multiple ONU cases, such short filter lengths thus result in the extremely strong crosstalk effect experienced by ONU2. It has been shown [18] that for multiple ONU cases, spectral location-independent ONU performance is still obtainable when filter lengths ($\text{filter length} = \text{tap count}/\text{M}$) are >8 and the alpha parameter values are <0.05.

V. CONCLUSIONS

A novel hybrid OFDM-DFMA PON has been proposed and investigated, for the first time, where multiple independent OFDM channels are multiplexed using ONU-embedded dynamically reconfigurable and adaptive digital filters, and simultaneously recovered in the OLT by a single FFT operation. An analytical theoretical hybrid OFDM-DFMA PON model has been developed to give an in-depth understanding of the proposed technique, and extensive numerical simulations of upstream hybrid OFDM-DFMA transmission performances have been investigated in representative 25km SSMF IMDD PON systems. It has been shown that the proposed technique greatly relaxes filter DSP complexity and improves PON performance flexibility and robustness because of its insensitivity to filter-induced signal distortions and system nonlinearity. Moreover, the numerical results have also demonstrated that the hybrid OFDM-DFMA PON can increase the differential ONU launch power dynamic range by 16dB compared to the DFMA PONs. The proposed technique may provide a valuable solution for practical implementation in 5G networks.

To verify the proposed hybrid OFDM-DFMA technique and the theoretical predictions presented in this paper, experimental investigations are currently being undertaken in our research lab, and corresponding results will be reported elsewhere in due course.

REFERENCES

[1] I. Tomkos, F. Effenberger, and J.-K. K. Rhee, "Introduction to the special issue on optical networking for 5G mobile and wireless communications," *J. Opt. Commun. Netw.*, vol. 8, no. 12, p. FGM1, Dec. 2016.

[2] J. S. Wey and J. Zhang, "Passive optical networks for 5G evolution," in *Broadband Access Communication Technologies XII*, vol. 10559, p. 22, 2018.

[3] L. Barona López, Á. Valdivieso Caraguay, M. Sotelo Monge, and L. García Villalba, "Key technologies in the context of future networks: operational and management requirements," *Futur. Internet*, vol. 9, no. 1, p. 1, Dec. 2016.

[4] J. Kani et al., "Flexible access system architecture (FASA) to support diverse requirements and agile service creation," *J. Light. Technol.*, vol. 36, no. 8, pp. 1510–1515, Apr. 2018.

[5] A. Otaka, J. Terada, J. Kani, and K.-I. Suzuki, "Solutions for future mobile fronthaul and access-network convergence," *J. Light. Technol.* Vol. 35, Issue 3, pp. 527-534, vol. 35, no. 3, pp. 527–534, Feb. 2017.

[6] X. Liu and F. Effenberger, "Emerging optical access network technologies for 5G wireless," *J. Opt. Commun. Netw.*, vol. 8, no. 12, p. B70, Dec. 2016.

[7] Abbas HS, Gregory MA. "The next generation of passive optical networks: A review," *Journal of Network and Computer Applications*, 2016, http://dx.doi.org/10.1016/j.jnca.2016.02.015i.

[8] H. F. Arrano and C. A. Azurdia-Meza, "OFDM: today and in the future of next generation wireless communications," *IEEE Central America and Panama Student Conference (CONESCAPAN)*, pp. 1–6. 2016.

[9] R. Nath Mitra and D. P. Agrawal, "5G mobile technology: A survey," *ICT*

Express, vol. 1, pp. 132–137, 2015.
[10] K. Kanonakis *et al.*, "An OFDMA-based optical access network architecture exhibiting ultra-high capacity and wireline-wireless convergence," *IEEE Commun. Mag.*, vol. 50, no. 8, pp. 71–78, Aug. 2012.
[11] N. Cvijetic, "OFDM for Next-Generation Optical Access Networks," *J. Light. Technol.*, vol. 30, no. 4, pp. 384–398, Feb. 2012.
[12] S.-Y. Jung, C.-H. Kim, S.-M. Jung, and S.-K. Han, "Optical pulse division multiplexing-based OBI reduction for single wavelength uplink multiple access in IM/DD OFDMA-PON," *Opt. Express*, vol. 24, no. 25, p. 29198, Dec. 2016.
[13] C. Zhang, W. Zhang, C. Chen, X. He, and K. Qiu, "Physical-enhanced secure strategy for OFDMA-PON using chaos and deoxyribonucleic acid encoding," *J. Light. Technol.*, vol. 36, no. 9, pp. 1706–1712, May 2018.
[14] R. Giddings, "Real-time digital signal processing for optical OFDM-based future optical access networks," *J. Light. Technol*. Vol. 32, Issue 4, pp. 553-570, vol. 32, no. 4, pp. 553–570, Feb. 2014.
[15] X. Zhang, C. Zhang, C. Chen, W. Jin and K. Qiu, "Non-optical carrier SSB-OFDM PONs with the improved receiver sensitivity and potential transmission nonlinearity tolerance," *IEEE Photon. J.*, vol. 9, no. 1, Feb.2017, Art. no. 7900910.
[16] W. Zhang, C. Zhang, C. Chen and Kun Qiu, "Experimental demonstration of security-enhanced OFDMA-PON using chaotic constellationc transformation and pilot-aided secure key agreement", *J. Light. Technol.*, vol. 35, no. 9, pp. 1524-1530, May 2017.
[17] T. Wu, C. Zhang, C. Chen, H. Hou, H. Wei, S. Hu and K. Qiu, "Security enhancement for OFDM-PON using Brownian motion and chaos in cell", *Opt. Express*, vol. 26, no. 18, pp.22857-22865, Sept. 2018.
[18] M. Bolea, R. P. Giddings, M. Bouich, C. Aupetit-Berthelemot, and J. M. Tang, "Digital filter multiple access PONs with DSP-enabled software reconfigurability", *J. Opt. Commun. Netw*, vol. 7, no. 4, pp. 215-222, Apr. 2015.
[19] X. Duan, R. P. Giddings, S. Mansoor, and J. M. Tang, "Experimental demonstration of upstream transmission in digital filter multiple access PONs with real-time reconfigurable optical network units," *J. Opt. Commun. Netw.*, vol. 9, no. 1, p. 45, Jan. 2017.
[20] C. Zhang, Y. Yan, T. Wu, X. Zhang, G. Wen, and K.Qiu, "Phase masking and time-frequency chaotic encryption for DFMA-PON", *IEEE Photon. J.*, vol.10, no. 4, Aug. 2018, Art. no. 7203009.
[21] X. Q. Jin, R. P. Giddings, E. Hugues-Salas, and J. M. Tang, "Real-time experimental demonstration of optical OFDM symbol synchronization in directly modulated DFB laser-based 25km SMF IMDD systems," *Opt. Express*, vol. 18, no. 20, 2010.
[22] B. Farhang-Boroujeny, "OFDM versus filter bank multicarrier", *IEEE Signal Process. Mag.*, pp.92-112, May 2011.
[23] Y. Dong, E. Al-Rawachy, R. P. Giddings, W. Jin, D. Nesset, and J. Tang, "Multiple channel interference cancellation of digital filter multiple access PONs," *J. Light. Technol*., vol. PP, no. 99, p. 1, 2016.
[24] X. Q. Jin and J. M. Tang, "Experimental investigations of wavelength spacing and colorlessness of RSOA-based ONUs in real-time optical OFDMA PONs", *J. Light. Technol*., vol. 30, no. 16, pp. 2603-2609, 2012.
[25] R. A. Shafik, M. S. Rahman and A. R. Islam, "On the extended relationships among EVM, BER and SNR as performance metrics," *International Conference on Electrical and Computer Engineering*, Dhaka, pp. 408-411, 2006.
[26] X. Q. Jin, J. Groenewald, E. Hugues-Salas, R. P. Giddings, and J. M. Tang, "Upstream power budgets of IMDD optical OFDMA PONs incorporating RSOA intensity modulator-based colorless ONUs," *J. Light. Technol*., vol. 31, no. 12, pp. 1914–1920, 2013.